Inorganic Chemistry

Article

pubs.acs.org/IC

High Dilution of Anionic Vacancies in $Sr_{0.8}Ba_{0.2}Fe(O,F)_{\sim 2.5}$

Mihai Sturza,[†] Sylvie Daviero-Minaud,[†] Marielle Huvé,[†] Nicolas Renaut,[†] Nicolas Tiercelin,[‡] and Olivier Mentré[†,*]

[†]Université Lille Nord de France, UCCS, CNRS UMR 8181, ENSCL-USTL, Villeneuve d'Ascq, France

[‡]International Associated Laboratory LEMAC: IEMN, UMR CNRS 8520, PRES Lille Nord de France, EC Lille, Villeneuve d'Ascq, France

Supporting Information

ABSTRACT: The $(Ba,Sr)FeO_{3-\delta}$ system is known for its strong tendency for oxygen and vacancies to order into several forms including fully ordered pseudobrownmillerites, hexagonal perovskites with segregation of the vacancies in particular anionic layers and low deficient (pseudo)cubic compounds (generally $\delta < 0.27$, $Fe^{3/4+}$). We show for the first time, using a simple chemical process, the easy access to a large amount of vacancies ($\delta \approx 0.5$, Fe^{3+}) within the room-temperature stable tetragonal (pseudocubic) $Sr_{0.8}Ba_{0.2}FeF_{\sim 0.1}(O,F)_{\sim 2.5}$. The drastic effect of the incorporation of a minor amount of fluoride passes through the repartition of local O/F/□ constraints shifting the tolerance factor into the pseudocubic range for highly deficient compounds. It is stable up to 670 K, where an irreversible reoxidation process occurs, leading to the cubic-form. The comparison with the cubic oxide $Sr_{0.8}Ba_{0.2}FeO_{\sim 2.7}$ shows the increase of the resistivity (3D-VRH model) by two decades due to the almost single valent Fe^{3+} of the oxofluoride. In addition, the G-type magnetic ordering shows relatively weak moment for Fe^{3+} cations ($M_{Fe} \approx 2.64(1)$ μB at room temperature) attributed to incoherent magnetic components expected from local disorder in such anionic-deficient compounds.

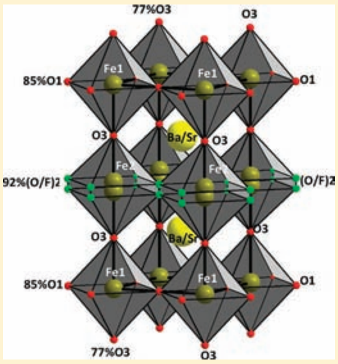

INTRODUCTION

The oxygen dissolution in solid oxides is responsible for complex transport and magnetic phase diagrams at the basis of most of the modern solid state sciences. In the broad series of perovskite compounds, the $BaMO_{3-\delta}$ terms (M = Mn, Fe, Co) show the greatest structural diversity versus the oxygen nonstoichiometry since anionic vacancies likely incorporate or eventually order in particular deficient $[BaO_{3-x}]$ layers which regulate the stacking between hexagonal (h) and cubic (c) layers. Therefore a number of distinct polytypes can be stabilized tuning the *redox* properties of the materials. Hence, in addition to its monodimensional 2H-form,[1] at least seven $BaMnO_{3-\delta}$ forms can be stabilized: 15R, 8H, 9R, 6H′, 10H, 4H, with different h/c ratio and sequence. It has been stated to respect to a preference of vacancies for face-sharing h-layers and for the prevalence of Mn_2O_{9-x} units at high vacancies concentrations.[2,3] Increasing the amount of vacancies leads to an ordering in the recent 4H-$BaMnO_{2+x}$ prepared by topotacic reduction.[4] In the M = Co case, starting from the low deficient 2H-form, oxygen vacancies preferentially agglomerate in the c-$[BaO_2]$ layers leading to the 5H/12H-polytypes[5,6] formed of trimers/tetramers with terminal CoO_4 tetrahedra. Structural rearrangements into new derivate-forms are reached by the incorporation of halides (X = F,Cl) preferentially in deficient h-[BaOX] layers.[7,8] Also, the possibility to increase δ up to ~0.8 (close to 1/3 of vacancies) lead to disordered $BaCoO_{\sim 2.2}$ cubic-phases.[9]

This stability seems inherent to cobalt-based perovskites since $Ba_{0,5}Sr_{0,5}Co_{0,8}Fe_{0,2}O_{3-\delta}$ (BSCF)[10,11] also was shown to possess high concentration of vacancies ($\delta \approx 0{,}7$) by means of Rietveld refinement and maximum entropy method (MEM) from neutron and synchrotron X-ray diffraction data. This high oxygen deficiency is at the origin of the great electrochemical properties of BSCF as cathode materials in SOFCs.[12,13]

In the iron case concerned here, oxygen defects have a great tendency for ordering, considering the progressive passage from the 6H-$BaFeO_{3-\delta}$ (weak δ values)[14] to the ordered monoclinic-distorted $BaFeO_{2.5}$ with only c-layers. Intermediate cubic deficient phases have also been reported for $0.44 < \delta < 0.5$, but their stabilization involves meticulous synthesis, using highly "reactive" precursors and a severe control of the heating/cooling treatments and of the working atmosphere.[15] As a matter of fact, during the recent reinvestigation of the $Sr_xBa_{1-x}FeO_{3-\delta}$ only the introduction of smaller Sr^{2+} for Ba^{2+} yields the cubic compound after thermal treatments in flowing air and oxygen atmospheres, this latter leading to $0.10 < \delta < 0.27$, depending on x. Similar $Sr_xBa_{1-x}FeO_{3-\delta}$ samples treated under N_2 lead to either the monoclinic, either the brownmillerite-like $AFe^{3+}O_{2.5}$ within ordered materials.[16] The fluorination of these samples by low-temperature thermal treatment using polyvinylidenefluoride results in the cubic $AFeO_2F$ (A = Sr/Ba) with Fe^{3+} only but no significant amount of vacancies.[17,18] The Sr-rich area of the diagram is all the more interesting since an evolution of the oxygen-vacancies ordering has been stabilized at room temperature in the series

Received: July 1, 2011
Published: November 10, 2011

Sr$_n$Fe$_n$O$_{3n-1}$ with discrete values for n (n = 2,4,8, and ∞) which leads to brownmillerite-derivatives[19] and only high temperature in equilibrium with air creates highly deficient pseudocubic SrFeO$_{3-\delta}$ phases (δ = 0.44 at 1273 K).[20] One should also note recent results on the topotactic reduction of A(Fe/M)O$_{3-\delta}$ (A = Sr, Ca, Ba ; M = Co, Mn) at moderate temperature by highly reactive hydrides leading to tetragonal AFeO$_2$ with layers of planar square Fe^{2+}.[21−24]

It results that the combination of both a cubic (or pseudocubic) symmetry with a large dilution of vacancies (δ = 0.5) is hardly reachable and has never been fully characterized yet, while their homogeneous repartition in the structure is topical, at least for electrochemical properties. Here we show that the introduction of a small amount of F$^-$ in the sample, using our synthesis method, enables to reach such compounds, in which the octahedral coordination should be mainly lost because of the high δ amount. We examine the (Ba,Sr)FeO$_{3-\delta}$F$_y$ phase-diagram, redox titration, powder-X-ray and neutron diffraction, thermal analyses and magnetic characterizations.

■ EXPERIMENTAL SECTION

Black polycrystalline samples of Sr$_x$Ba$_{1-x}$FeF$_{0.2}$O$_{3-\delta}$ ($0 \leq x \leq 1$) and Sr$_{0.8}$Ba$_{0.2}$FeF$_y$O$_{3-\delta}$ ($0 \leq y \leq 1$) have been obtained through solid-state reaction using stoichiometric mixtures of BaO$_2$ (Aldrich 95%), SrO$_2$ (Aldrich 95%), Fe$_2$O$_3$ (Aldrich 99%), BaF$_2$ (Aldrich 99%), and SrF$_2$ (Aldrich 99%) as starting materials. The mixtures were ground in an agate mortar and placed in closed (but not sealed) gold-tubes. The samples were subsequently heated for 48 h at 1223 K for Sr$_x$Ba$_{1-x}$FeF$_{0.2}$O$_{3-\delta}$ ($0 \leq x \leq 1$), and then quenched to room temperature. In the line of the phase diagram corresponding to Sr$_{0.8}$Ba$_{0.2}$FeF$_y$O$_{3-\delta}$ ($0 \leq y \leq 1$) some samples were prepared and quenched in air and other were slow cooled in their tubes for comparison.

XRD profiles were recorded with a Bruker D8 diffractometer, Cu$_{K\alpha}$ radiation. High temperature X-ray diffraction (HT-XRD) experiments were carried out on Sr$_{0.8}$Ba$_{0.2}$FeF$_{0.1}$O$_{3-\delta}$ and Sr$_{0.8}$Ba$_{0.2}$FeO$_{3-\delta}$ powder from room-temperature up to 1273 K using an Anton Paar HTK 1200N chamber under flowing air. Powder ND analyses were performed on Sr$_{0.8}$Ba$_{0.2}$FeF$_{0.1}$O$_{2.477}$ at the Laboratoire Léon-Brillouin (LLB) Saclay, France at room temperature, using the 3T2 diffractometer (λ = 1.2254 Å). Powder-XRD and ND data were analyzed with the Rietveld[25] method using the FULLPROF 2000 suite.[26] The background was simulated by punctual values, while the peak-profile was fitted using a pseudo-Voigt function.

Electron diffraction (ED) patterns were obtained on a FEI Technai G220 transmission electron microscope equipped with a precession system. The material was crushed and dispersed on a holey carbon film deposited on a Cu grid.

Thermogravimetric analysis (TGA) and differential thermal analysis (DTA) were carried out using a combined TG-DTA 92−1600 SETARAM analyzer. Successive heating/cooling cycles were performed using a rate of 5 °C/min.

The oxidation state for iron was determined by a red-ox titration method. The samples were dissolved in a H$_3$PO$_4$/H$_2$SO$_4$ acidic medium with an excess of Mohr-salt ((NH$_4$)$_2$Fe(SO$_4$)$_2$·6H$_2$O) under flowing argon. The formal Fe^{4+} reacts with Fe^{2+} leading to Fe^{3+} formation. The amount of remaining Fe^{2+} ions is determined by back-titration with a 0.1 M KMnO$_4$ solution.

Fluoride titration and atomic composition was performed on selected powder samples after dissolution of the compounds, using F specific electrode at the Service Central d'Analyses du CNRS, 69360 Solaize, France. Two samples have been analyzed: the "as-prepared" Sr$_{0.8}$Ba$_{0.2}$FeF$_{0.1}$O$_{3-\delta}$ and the same sample reheated at 1173 K for 24 h, which shows a fluoride departure after heating as detailed below.

Magnetization cycles and magnetization versus temperature were measured using an ADE EV9 vibrating sample magnetometer (VSM). Samples were heated during the measurements via a heated gas flow in a thermally isolated tube. Dry air was used to prevent unwanted reduction of the samples at higher temperatures. For low temperature DC magnetization was measured in a SQUID magnetometer, in the range 2 to 300 K under an applied magnetic field of 200 Oe. The field dependence of the magnetization at 2 K was carried out in the range 0−50 kOe.

The variations in resistivity obtained while heating and cooling between 10 and 300 K were measured using a standard four probes cell, in vacuum (10^{-4}−10^{-5} mbar). The mixture of staring compounds were pressed into bars, densified using an isostatic press and heated at the synthesis temperature in order to increase the compactness up to 80%. The reaction was performed in closed gold-tube for both the oxide (slow-cooling) and the oxofluoride (quenching) samples, similarly to the powder syntheses.

■ RESULTS AND DISCUSSION

The phase compositions within the Sr$_x$Ba$_{1-x}$FeF$_{0.2}$O$_{3-\delta}$ ($0 \leq x \leq 1$) system are listed against the observed crystal structures in Table 1. These results mainly concern samples prepared in closed gold-tubes at 1223 K, after quenching to room temperature (denoted as-prepared) while some nonfluorinated samples correspond to results from ref 16 after preparation in air.

In the barium-rich zone of the diagram (x = 0−0.2), the fluorinated-hexagonal-perovskites (FHP), which adopt either the 15R (= [cchch]$_3$ stacking sequence) either the 6H (= [chcchc] stacking sequence) types are obtained as reported in refs 27 and 28. Briefly, we have shown in these compounds a net preference of F$^-$ for particular sites of the fluorinated/disordered [BaO$_{3-x}$F$_y$] hexagonal layers while a drastic O^{2-}/F$^-$/$\square$ reorganization occurs upon heating. In their as-prepared state, the mean iron valence is close to +3, which reinforces the robust antiferromagnetism ($T_N \approx$ 700K) observed in these compounds despite their unfavorable hexagonal stacking. It is clear that the occurrence of h-layers in these region is guided by the tolerance factor $\boldsymbol{t}$ (= $(r_A + r_O)/\sqrt{2}(r_B + r_O)$) close to 1.05 (calculated for A = Ba^{2+} and B = Fe^{3+}). The ratio y of incorporated F$^-$ delimits a solid solution domain ($0.15 < y < 0.35$) for the 15R compound and ($0.15 < y < 0.25$) for the 6H. It is rather extended comparatively to the cubic (Sr-rich zone) domains investigated here ($y \approx 0.1$).

Hence only the Sr$_{0.8}$Ba$_{0.2}$FeF$_{0.1}$O$_{3-\delta}$ composition revealed the existence of a pure tetragonal (pseudocubic) phase, using our synthesis protocol. The fine-tuning of x and y systematically yielded a mixture of phases, sometimes including SrF$_2$, which clearly reveals the limits of the F$^-$ dilution in pseudocubic phase using our high temperature protocol. The Figure 1 shows the identification of the pure tetragonal phase for y = 0.1. Clearly, this unreported compound is stabilized by incorporation of F$^-$ since (i) nonfluorinated samples lead either to a brownmillerite/BaFe$_2$O$_4$/SrBaFe$_4$O$_8$ mixture either to the cubic SrFeO$_{3-\delta}$ form depending on the preparation method. (ii) Only the quenched samples show evidence for the tetragonal phase, see Table 1. Hence, the comparison between the single-phase tetragonal Sr$_{0.8}$Ba$_{0.2}$FeF$_{\sim 0.1}$O$_{3-\delta}$ and the cubic Sr$_{0.8}$Ba$_{0.2}$Fe O$_{3-\delta}$ deserves interest in terms of their anionic sublattice, considering the narrow range of existence of the former. Thus, on the basis of our previous evidence of the strong anionic disorder created by F$^-$ (ratio $y \approx$ 0.15−0.35) in the fluorinated hexagonal Fe-perovskites, the influence of the minor amount (ratio $y \approx 0.1$) in pseudocubic structures is topical.

Structural Analysis. *Cubic-Sr$_{0.8}$Ba$_{0.2}$FeO$_{2.68}$.* The redox titration of the cubic phase after slow-cooling of the gold tube indicates δ=0.32 (Fe$^{+3.37}$). Its XRD and ED pattern indicates a

Table 1. Phases Indentified in the Investigation of the $Sr_xBa_{1-x}FeF_yO_{3-\delta}$ System (Closed Golden Tube at 950 °C, after Quenching in Air)[a]

x	0	0.2	0.4	0.5	0.6	0.7	0.8				1
							closed golden tube		air samples		
y							quench	slow cooling	quench	slow cooling	
0	MC + C	6H + C + BF	C[14]	C[14]	C[14]	C[14]	BR + BF + SBF	**C**	BR + SBF	C[16]	T1[16]
0.05	6H	6H + C									
0.1	6H	6H + C					**T2**	C + SrF_2	C + SrF_2	C + SrF_2	
0.15	15R	6H					T + SrF_2 + SBF				
0.2	15R	6H	6H + T	6H + T + SBF	6H + T	T + SBF	T + SrF_2 + SBF	C + SrF_2 + SBF			BR + SrF_2
0.25	15R	6H									
0.3	15R	6H + 15R					T + SrF_2 + SBF	C + SrF_2 + SBF			
0.35	15R	6H + 15R									
0.4	15R + BaF_2 + BF	6H+ 15R+ BF						C + SrF_2 + SBF			

[a] The compounds, which correspond to $y = 0$, $x = 0.4-0.7$, were prepared in air from ref 16. T1= tetragonal ($I4/mmm$, a = 10.9341(6) Å, c = 7.7024(5) Å) MC = monoclinic, C = cubic, T2 = tetragonal ($P4/mmm$, a = 3.92688(4) Å, c = 7.9648(3) Å), BR = brownmillerite, BF = $BaFe_2O_4$, SBF = $SrBaFe_4O_8$. The compounds in red are at the basis of this work.

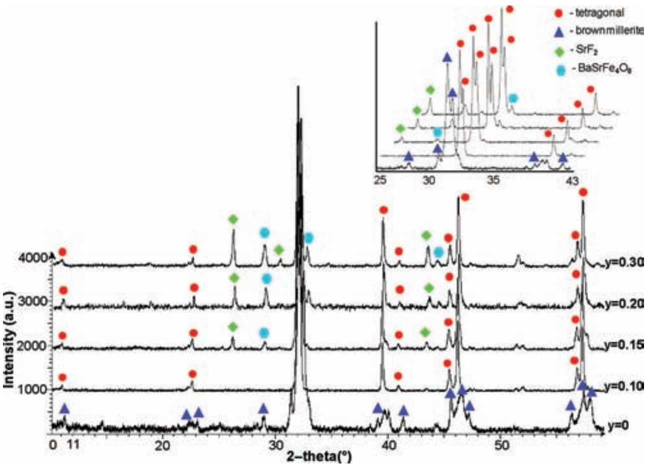

Figure 1. XRD patterns of $Sr_{0.8}Ba_{0.2}FeF_yO_{3-\delta}$ with y = 0−0.3 synthesized in closed golden tube at 950 °C and quenched to RT. A single phase is obtained for y = 0.1.

primitive cubic cell ($Pm\bar{3}m$ space group) with a = 3.8862(1) Å. From the Rietveld refinement, the corner sharing $Fe^{3+}O_6$ (66%) and $Fe^{4+}O_5$ (33%) polyhedra are formed of Fe−O bonds of 1.9432(5) Å. (see Figure.2c and Tables 2 3.) leading to the bond valence sum (BVS) calculated from Brese and O'Keeffe data of +3.36 (for $Fe^{3+}O_6$). Slow cooled air-prepared compounds also yield a cubic-phase with formula $Sr_{0.8}Ba_{0.2}Fe^{+2.9}O_{2.98}$ according to our redox titration similarly to results of ref 16..

Tetragonal- $Sr_{0.8}Ba_{0.2}FeF_{0.06}O_{2.48}$. our elemental analysis (F/Ba/Sr/Fe) combined with redox titration leads to the formula: $Sr_{0.8}Ba_{0.2}Fe^{+3.04}F_{0.06}O_{2.49}$ which suggest that contrarily to the fluorinated hexagonal phases, the fluoride incorporation is significant but not total (experimental ratio y = 0.1). By comparison to other experimental procedures leading to more oxidized cubic compounds or multiphased samples (see previous section and Table 1), it is noteworthy that the quenching of the samples is necessary to stabilize the tetragonal reduced form. The Figure 3a show the XRD patterns of the stabilized oxofluoride which can be indexed in a pseudocubic (tetragonal) unit cell, a = 3.92688(4) Å, c = 7.9648(3) Å. Evidences of weak $00l$ reflexions comfort the c-doubling while the spitting of certain lines shows the divergence the tetragonal distortion ($c > 2 \times a$). This c-doubling is observed by ED, see inset of Figure 3a. The ND study at room temperature was performed for an accurate characterization of the anionic sublattice. The ND data also show heavy magnetic contributions which correspond to the setting of an AFM ordering even at room temperature. The crystal structure was refined in the $P4/mmm$ space group. The atomic positions are listed in Table 2. Table 3 lists selected interatomic distances. As shown in the Figure 2b, from Fourier-difference maps, the central oxygen atom O,F2 and Fe2 atoms have been split into ($4i$) positions leading to final reliability factors: profile R_p= 10.5%, R_{wp}= 9.29%, R_{exp}= 3.12%; structural R_{Bragg} = 3.33%, R_F = 3.27%, R-magn.=3.62% (see Supporting Information Figure S2). Another model using anisotropic thermal displacements for Fe2 was also considered leading to similar R values. However the split of Fe2 better matches the Fourier-difference map. The occupancies of the three independent oxygen O1 (site 2f), O,F2 (site $4i$), and O3 (site $2g$) were refined to Occ(O1) = 85%; Occ(O2) = 46% (= 92% for the ideal position), and Occ(O3) = 77%. It gives the final formula $Sr_{0.8}Ba_{0.2}Fe^{+3.02}$-$F_{0.06}O_{2.48}$ after fixing the F^- content accordingly to our chemical titration.

We suggest the segregation of F^- in the central $(FeO_{1.72}F_{0.12})$ plane on the basis of results by Alekseeva et al.[29] to explain the tetragonal distortion of the structure of the $Sr_2MnGa(O,F)_6$ oxofluorides where fluorine occupies the central $(GaO_{1.5}F_{0.5})$ plane. Then, in our compound, F^- anions would drive the lattice distortion and create local defects responsible for the (O,F) and Fe2 splitting. The analysis of bond distances indicates a distribution of bonds around Fe2 (Fe2−(O,F)2 = 1.96−1.99 Å and Fe2−O3 = 1.80−2.16 Å, comparatively to Fe1−O1 = 1.94 Å and Fe1−O3 = 1.98 Å). First, the splitting of

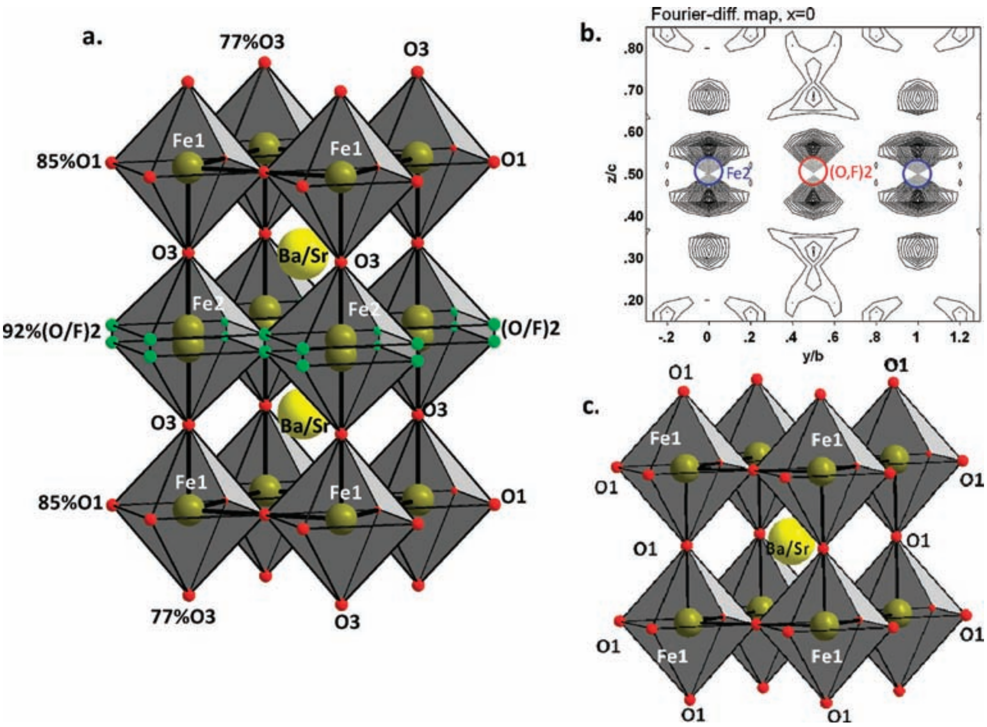

Figure 2. View of the polyhedral structure of (a) $Sr_{0.8}Ba_{0.2}Fe^{+3.02}F_{0.06}O_{2.48}$ and (c) $Sr_{0.8}Ba_{0.2}FeO_{3-\delta}$. (b) Fourier-difference map of the (0,*y*,*z*) layer with evidence of the split of Fe2 and (O,F)2 in $Sr_{0.8}Ba_{0.2}Fe(O,F)_{\sim 2.5}$.

Table 2. Atomic Coordinates and Isotropic/Equivalent Thermal Displacement Parameters for $Sr_{0.8}$ $Ba_{0.2}Fe^{+3.02}F_{0.06}O_{2.48}$ from PND Data (Bragg R-Factor = 3.33%; Rf-factor = 3.27%; R-mag = 3.62%, R_p = 10.5%, R_{wp} = 9.29%, R_{exp} = 3.12%) and $Sr_{0.8}Ba_{0.2}Fe^{+3.36}O_{2.68}$ from XRD Data (Bragg R-factor = 4.29%; Rf-factor = 4.10%, R_p = 3.08%, R_{wp} = 3.96%, R_{exp} = 3.23%, χ^2 = 1.51) for $Sr_{0.8}Ba_{0.2}FeO_{3-\delta}$

atom	Wyck./Occ.	*x*	*y*	*z*	U_{iso}/equiv (Å^2)
		$Sr_{0.8}Ba_{0.2}Fe^{+3.02}F_{0.06}O_{2.48}$			
Sr1	2*h*/0.8	1/2	1/2	0.2680(3)	0.0153(3)
Ba1	2*h*/0.2	1/2	1/2	0.2680(3)	0.0153(3)
Fe1	1*a*/1	0	0	0	0.0348(6)
Fe2	2*g*/0.5	0	0	0.4776(4)	0.0080(5)
O1	2*f*/0.85(3)	1/2	0	0	0.0601(14)
(O,F)2[a]	4*i*/0.46(2)	1/2	0	0.4755(4)	0.0097(7)
O3	2*g*/0.77(5)	0	0	0.2498(7)	0.0298(11)
		$Sr_{0.8}Ba_{0.2}Fe^{+3.36}O_{2.68}$			
Sr1	1*b*/0.8	1/2	1/2	1/2	0.0251(5)
Ba1	1*b*/0.2	1/2	1/2	1/2	0.0251(5)
Fe1	1*a*/1	0	0	0	0.0284(8)
O3	3*d*/0.893(4)	0	0	1/2	0.045(3)

[a] The position is occupied together by oxygen and fluorine: 0.03F + 0.43O

Table 3. Selected Bond Distances (Å) for $Sr_{0.8}$ $Ba_{0.2}$-$Fe^{+3.02}F_{0.06}O_{2.48}$ (from PND Data) and $Sr_{0.8}Ba_{0.2}Fe^{+3.36}O_{2.68}$ (from XRD Data)

atoms	*d* (Å)
$Sr_{0.8}Ba_{0.2}Fe^{+3.02}F_{0.06}O_{2.48}$	
Fe1−O3 (×2)	1.982(3)
Fe1−O1 (×4)	1.9634(5)
Fe2−O3 (×2)	1.808(3)−2.164(4))
Fe2−(O,F)2 (×4)	1.963(5)−1.998(3))
$Sr_{0.8}Ba_{0.2}Fe^{+3.36}O_{2.68}$	
Fe1−O1 (×6)	1.9432(5)

both the Fe2 and (O,F)2 sites is presumably correlated, and it is probable that the (a,b) planar coordination remains but shifted along c. Then the creation of vacancies around Fe1 (~25% of vacancies on the axial−O1 site) within a regular polyhedron is compensated on Fe2 (~8% of vacancies on the axial-(O,F)2) site by the splitting of axial bonds into a short and a longest one. It acts such that both Fe1 and Fe2 would match a coordination compatible for Fe^{3+}.Taking into consideration the refined concentration of vacancies on each site, the average coordination of iron centers are $Fe1O^{ax}_{1.54}O^{eq}_{3.4}$ and Fe2-$O^{ax}_{1.54}(O,F)^{eq}_{3.68}$ which leads to the average BVS of +2.83 and 3.04 respectively good agreement with the mean trivalent state of iron.

Also, the mean elongation of in-plane Fe2-(O,F)2 bonds play in favor of F^- presence in this position. Clearly Fe2−F bonds are expected to create strong local constraints with respect to the F^- bond valence sum (BVS). The BVS being commonly defined by $S_{ij} = \Sigma_j \exp[(R_{ij} - d_{ij})/0.37]$,[30] it appears that the replacement of O^{2-} ($S = -2$, $R_{O-FeIII} = 1.759$) for F^-($S = -1$, $R_{F-FeIII} = 1.67$) is expected to elongate the mean Fe---F distance. Of course a statistic repartition of fluorides on O1, O2, and O3 positions cannot be fully excluded.

Pseudo-Ordering of the Anionic Vacancies. The x = 0.8 ratio is well adapted to stabilize the pseudocubic edifice since the tolerance factor $\boldsymbol{t}$ (= $(r_A + r_O)/\sqrt{2}(r_B + r_O)$) is calculated to 0.999 for an ideal $Ba_{0.2}Sr_{0.8}Fe^{3+}O_{3-\delta}$ compound, neglecting the necessary amount of vacancies ($\delta = 0.5 \rightarrow Fe^{3+}$). In real, the nonfluorinated $Sr_{0.8}Ba_{0.2}Fe^{+3.36}O_{2.68}$ cubic form is stabilized by the concomitant δ-effect (δ around 0.3) and the decrease of r_B increase ($rFe^{3+} > rFe^{4+}$). The increasing of δ in the fluorinated title compound is associated with a tetragonal

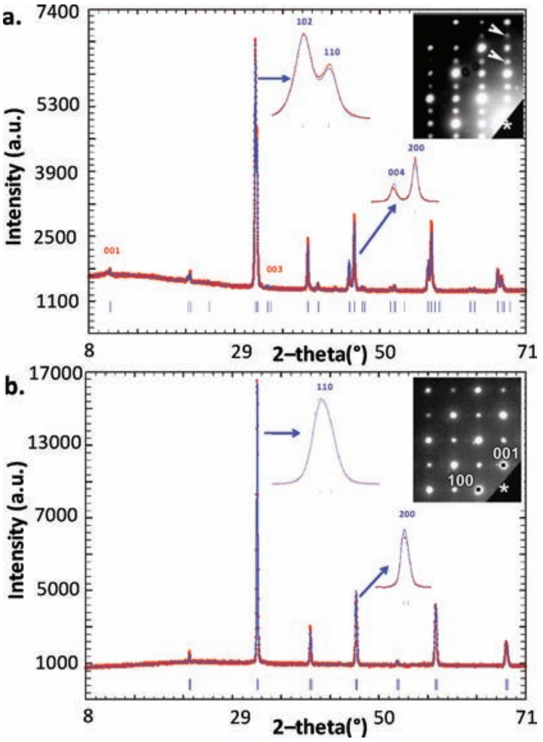

Figure 3. XRD patterns and ED images for (a) the tetragonal $Sr_{0.8}Ba_{0.2}FeF_{0.1}O_{3-\delta}$ phase with a unit cell 3.8,3.8,7.9 Å, (b) the cubic phase which result after heating the tetragonal compound with a unit cell 3.8, 3.8, 3.8 Å.

distortion expected for lower *t* values, in good agreement with the Fe^{4+} reduction into Fe^{3+} in the oxofluoride. One should also recall that in the Fe^{3+} perovskites an anionic ordering is generally observed, for example, in the brownmillerite or other $Sr_nFe_nO_{3n-1}$ derivatives.[19] In fact, a high concentration of disordered vacancies in the cubic phase only exist at high temperature.[20] According to our results, it is striking that the introduction of minor amount of F^- in the structure allows the stabilization of a high concentration of vacancies in $Sr_{0.8}Ba_{0.2}Fe^{+3.02}F_{0.06}O_{2.48}$ (~1/6 of the available sites) in a disordered manner. The Figure 4 shows the $[Ba(O,F)_{3-\delta}]$ anionic layers parallel to (112). Here raws of O1, (O,F)2, and (Ba/Sr/O3) alternate leading to two kinds of Ba−Ba separations depending on the concentration of the central anion. In fact, due to the cubic-close-packing of those layers the 3D anion/vacancies repartition is rather homogeneous. The effect of F^- is not fully understood yet, but at least can we propose a repartition of local constraints. Also, as reported for the fluorinated-hexagonal phases,[27] the effective reduction of Fe when F^- replaces O^{2-} plays in favor of an anion-deficient phase. Therefore, $Sr_{0.8}Ba_{0.2}Fe^{+3.04}F_{0.06}O_{2.49}$ presents a rare example of high concentration of disordered vacancies in a pseudocubic iron perovskite.

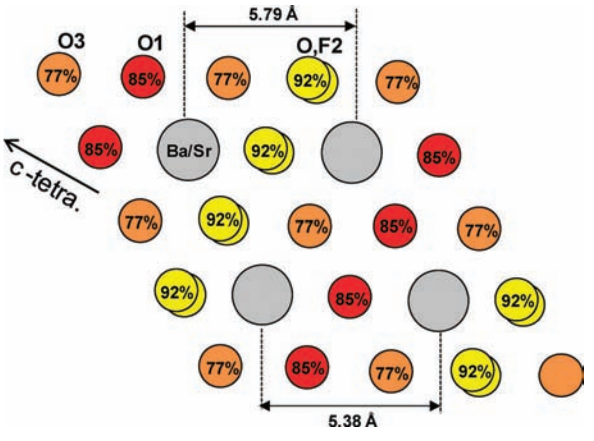

Figure 4. Scheme of the anionic distribution in closed-packed $[Ba(O,F)_{3-\delta}]$ layers parallel to (112) in the tetragonal cell in $Sr_{0.8}Ba_{0.2}FeF_{0.1}O_{3-\delta}$.

Thermal Stability. Recent studies have shown the great stability of F^- ions when incorporated in hexagonal layers of Fe-based perovskites. Typically, the 15*R*-fluorinated-hexagonal perovskite (15R-FHP) shows thermal stability above 1273K without significant fluoride loss. Such a rare behavior in the field of oxofluorides is made possible by the reversible reorganization of the hexagonal anionic array (O^{2-}, F^-, and vacancies) in which ideal sites for F^- exist but are displaced in-plane, while vacancies are created upon temperature.[27] Contrarily, cubic $(Ba/Sr)FeO_2F$ prepared after a topotactic fluorination route are metastable and yield $(Ba/Sr)F_2$ salts at moderate temperature (673 K).[16−18] This difference of behavior is probably related to the severe local constraints in the pseudocubic anionic subarray because of the replacement of O^{2-} by F^-. Clearly, even if strongly anion-vacant, the situation for the pseudocubic $Sr_{0.8}Ba_{0.2}Fe^{+3.02}F_{0.06}O_{2.48}$ is expected similar and the comparison of its thermal behavior comparatively to $Sr_{0.8}Ba_{0.2}Fe^{+3.37}O_{2.68}$ is of interest. In-situ high temperature XRD experiments for the fluorinated compound in air reveals a metastable character by an irreversible tetragonal → cubic transition around 620−673 K (see Supporting Information Figure S3a). After the first heating/cooling ramp, the lattice parameters finally coincide with those of the cubic oxide, which suggests the removal of main of the initial fluoride content (see Figure 5a). This compositional change was proved by the fluor titration of the as-prepared tetragonal phase, after a two-days thermal treatment at 1173 K in air ; it shows an evolution of the titrated F from $x = 0.06$ (as-prepared) to 0.03 (after treatment). Contrarily, the oxide $Sr_{0.8}Ba_{0.2}Fe^{+3.37}O_{2.68}$ shows the conservation of the cubic material on heating/cooling (see Supporting Information Figure S3b). The thermal gravimetric analysis under air for the tetragonal phase shows a broad oxidation peak from 620 to 770 K (from as-prepared to intermediate-oxidized states) (see Figure.5c),which accompanies a drastic lattice contraction up to the cubic transformation. It probably coincides with the main loss of fluoride. This oxidation is immediately followed by a monotone important reduction on heating and reoxidation on cooling. This general reduction at high temperature observed on all tested compounds is at the probable origin of the necessity for quenching samples to stabilize the oxygen-deficient oxofluoride. Accordingly to the TGA curve combined with the initial titration and elemental analysis the subsequent stages correspond to: as-prepared $Sr_{0.8}Ba_{0.2}Fe^{+3.02}F_{0.06}O_{2.48}$ (RT) → *intermediate*-oxidized $Sr_{0.8}Ba_{0.2}Fe^{+3.23}F_{0.03}O_{2.60}$ (770 K) → reduced $Sr_{0.8}Ba_{0.2}Fe^{+2.89}F_{0.03}O_{2.43}$ (1273 K) ↔ oxidized $Sr_{0.8}Ba_{0.2}Fe^{+3.27}F_{0.03}O_{2.62}$ (RT). We verified the iron valence after TGA that gives +3.29 in agreement with the TGA-expected +3.27 value. This complex behavior emphasizes the drastic role of a minor F^- amount. By comparison, starting from the initial $Sr_{0.8}Ba_{0.2}FeO_{3-\delta}$ the Fe valence reversibly changes between $Fe^{+3.37}$ at room temperature and $Fe^{+2.66}$ at 1273 K.

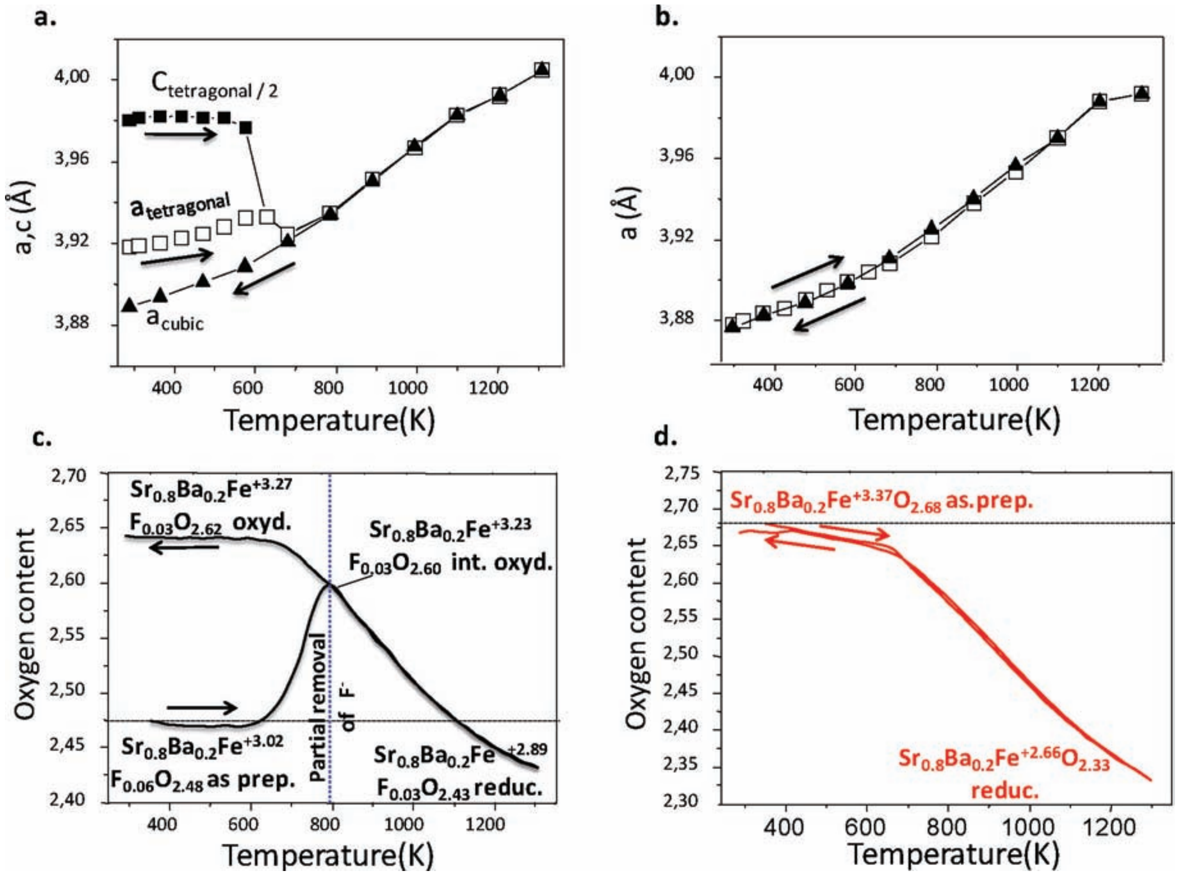

Figure 5. Evolution of the cell parameters functions of temperature for (a) the tetragonal $Sr_{0.8}Ba_{0.2}FeF_{0.06}O_{2.48}$ with tetragonal → cubic transformation at 670 K on heating. Above 670 K, it follows the evolution of the nonfluorinated cubic compound and comforts the removal of a significant part of the F^- content from 0.06 to 0.03 from chemical analyses (b) the cubic nonfluorinated $Ba_{0.2}Sr_{0.8}FeO_{2.68}$. The TGA curves under flowing air, under subsequent heating/cooling cycle, and the deduced formula from redox and fluor titrations are shown in panels c (note the oxidation reactions starting at 620 K) and d (monotone behavior).

Physical Properties. High-temperature M(T) measurements performed in air show a magnetic anomaly around 650 K, which merely coincides with the tetragonal to cubic transformation and reach a paramagnetic regime above 710−730 K, θ_{CW} = −996 K, μ_{eff} = 5.25 μB/Fe from data upon heating. From our thermal analysis, at this temperature the resulting valence should be dominated by trivalent species (predicted μ_{eff} = 5.39 $\mu B/Fe^{3+}$ in a spin-only approximation). Despite the relative imprecision on the linear regression in the high-temperature domain, the high magnitudes of θ_{CW} indicate strong AFM exchanges, as expected, since 180 °Fe^{3+}—O—Fe^{3+} superexchanges are predicted strongly antiferromagnetic.[31,32] We note the good concordance of our high-temperature (HT) and low-temperature (LT) data measured differently: LT using a SQUID under helium atmosphere and HT using a VSM magnetometer in air, Figure 6b. A weak anomaly is also detected at 130K on the $M/H(T)$ plot. The magnetization curves also show that below T_N, the AFM ordering is accompanied by a weak remanent moment of 7.10^{-3} and 2.10^{-3} μB/f.u. at 2 and 300K respectively, Figure 6c. It likely results from the interplay between various $Fe(O,F)_{6-x}$ polyhedra due to the large δ value and also from the minor but sensitive amount of Fe^{4+}, which could initiate FM exchanges. The true value for T_N is hardly estimable from $M(T)$ because of the prior transformation into the cubic phase, however it can roughly be estimated to 680−720 K according to comparable, but less deficient Fe^{3+} oxofluorides $BaFeO_2F$ (T_N = 645 K),[17] $SrFeO_2F$ (T_N = 685 K),[18] $Sr_{0.5}Ba_{0.5}FeO_2F$ (T_N = 670 K),[33] $PbFeO_2F$ (T_N > 500 K),[34] and 15R/6H $(Ba,Sr)FeO_{3-x}F_y$ ($T_N \approx$ 700 K).[28]

The magnetic structure has been refined from RT-PND data using the k = (1/2, 1/2, 0) propagation vector necessary to include the magnetic satellites (Supporting Information Figure S2). All magnetic satellites of (hk0) reflections are null, while the strongest magnetic lines corresponds to (001) + k (d_{hkl} = 4.55 Å). According to the dipolar spin-neutron interactions it involves magnetic moments parallel to the c-axis. Comparatively to the tetragonal (a, a, $c \approx 2a$) atomic period, it also involves a doubling of the magnetic lattice along a, while c is conserved. Several magnetic models have been tested and only the G-type AFM ordering allows to a simulation of magnetic contributions (R_{magn} =3.62%). For instance the C-type model leads to R_{magn} of 70%. In the G-type AFM, each Fe atom is antiferromagnetically coupled to its six nearest neighbors via intervening O (or F) atoms. The moments (∥c) were assumed similar in the two octahedral crystallographic positions Fe1 and Fe2, leading to 2.64(1) μ_B per Fe, see Figure 6a. In fact the amplitude of the ordered moments at RT appears much lower than expected from the moment reduction ($MFe^{3+} \approx 3.5\ \mu_B$ at RT for $T_N \approx$ 700 K, $T/T_N \approx$ 0.4) for S = 5/2 Brillouin curve, for example, in the oxides, such as $Sr_2Fe_2O_5$,[20] $Ca_2Fe_2O_5$,[35] $LaCa_2Fe_3O_8$, and $Ba_{1.6}Ca_{2.3}Y_{1.1}Fe_5O_{13}$,[36] all of them with ~180° Fe^{3+}—O—Fe^{3+} superexchanges and high T_N close to 700 K. Since PND measures only the long-range ordered

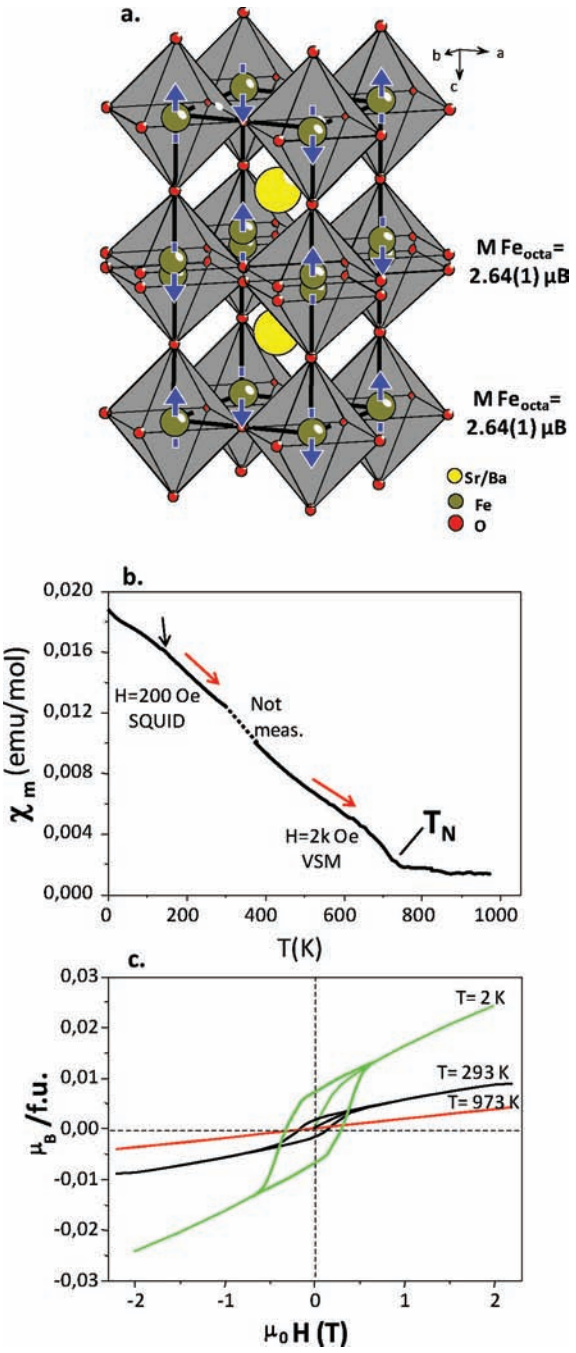

Figure 6. (a) the magnetic structure of $Sr_{0.8}Ba_{0.2}Fe^{+3.02}F_{0.06}O_{2.48}$ refined from RT-PND (R-mag = 3.78%) at 299 K. (b) Magnetic susceptibility versus temperature under an applied magnetic field of 200 Oe at low temperature (SQUID) and 2 K Oe at high temperature (VSM) for the $Sr_{0.8}Ba_{0.2}FeF_{0.06}O_{2.48}$ sample. The arrow indicates an anomaly at 130 K. (c) The magnetization curves at 2, 293, and 973 K.

magnetic component, the low moments observed for $Sr_{0.8}Ba_{0.2}Fe^{+3.02}F_{0.06}O_{2.48}$ can be attributed to the presence of local structural disorder (O/F, vacancies, and cationic shift), which could result in imperfect alignment of spins. Incoherent components in the (*a*,*b*) plane is then expected. Finally the magnetic anisotropy along *c* likely results from the lattice distortion but is hardly rationalizable in so-deficient phases since we have recently demonstrated the drastic effect of minor changes of the concentration of anionic vacancies on the orientation of the moments in $BaCoF_xO_{3-y}$ hexagonal perovskites.[37]

The transport properties have been measured on bars of the oxide and oxofluoride with a compacity greater than 80% for the oxide and the oxofluoride. Then, a contibution of grain boundaries is suspected but could be neglected from the qualitative viewpoint by comparison between the two compounds. $SrFeO_{3-\delta}$ is known to be metallic for $0 < \delta <$ ~0.15, while it is an insulator below Lebon et al.[38] Additionally Fe^{3+}/Fe^{4+} charge-ordering was detected for $\delta = 0.17$ but do not subsist above $\delta = 0.2$.[39] The increasing of δ up to 0.32 in $Sr_{0.8}Ba_{0.2}FeO_{2.68}$ falls in the insulating area, as clearly observed from the resistivity values (ρ = 40 Ω.cm at room temperature). It was not possible to fit $\rho(T)$ using an Arrhenius law, while by analogy with $SrFeO_3$[39] a Mott variable range hopping (VRH) model of hopping conduction ($\log(\rho)\alpha T^{-1/(D+1)}$) allows a good linearization using $T^{-1/4}$ ($D = 3$), see Figure 7. It indicates a three-dimensional hopping conduction between Anderson-localized states. For $Sr_{0.8}Ba_{0.2}Fe^{+3.02}F_{0.06}O_{2.48}$, the striking point lies in the increasing of ρ by 2 orders of magnitude compared to the oxide. It should mainly picture the nearly single valent state (Fe^{3+}) in the $Sr_{0.8}Ba_{0.2}Fe^{+3.02}F_{0.06}O_{2.48}$ assorted with longer interatomic separations compared to the mixed valent $Sr_{0.8}Ba_{0.2}Fe^{+3.37}O_{2.68.}$ On cooling, the oxofluoride shows an anomaly at 130 K reminiscent of its magnetic behavior. A 3D-VRH conduction model also matches our experimental results with two different slopes at both sides of the transition-point. Same results have been explained on the basis of the variation of the localization length for $SrFeO_{2.8}$.[39] The nature of the transition could be a charge ordering of weak amplitude due to the minor amount of Fe^{4+} dilute in the metal lattice, but the presence of F^- for O^{2-} could also play a role. This aspect will be examined in a further work.

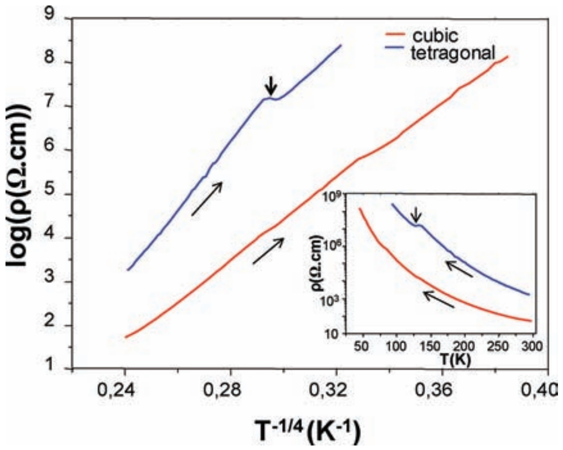

Figure 7. Evolution of resistivity plotted as a 3D-VRH conduction model for the tetragonal $Sr_{0.8}Ba_{0.2}FeF_{0.06}O_{2.48}$ and cubic sample $Sr_{0.8}Ba_{0.2}FeO_{2.68}$ in the domain de 10−300 K. The anomaly at 130 K is shown by an arrow.

■ CONCLUSION

We have demonstrated the ability to stabilize a large amount of oxygen vacancies in pseudocubic symmetry via an easy fluorination way. Only a minor amount of fluorides ($y \approx 0.1$) was incorporated in single-phased samples which enhance the drastic role of F^- by introducing local constraints, even at low dilution in the 3D-perovskite framework. The anionic vacancies are not fully disordered since the repartition between the three available anion sites is different. However it appears relatively homogeneous in regard to a three-dimensional scheme. Clearly the effect of both the fluor segregation in the more filled sites and the high amount of vacancies creates local constraints which stabilize the deficient tetragonal edifice. This "disorder" effect is also probed from the magnetic structure, in which the low observed magnetic moments on each Fe-site are explained by local magnetic inhomogeneity and subsequent incoherent magnetic components, which perturbate the ideal G-type AFM ordering. Having in mind the good mixed ionic/electronic transport of Fe-based perovskites (A-doped cubic stabilized $BaFeO_{3-\delta}$ phases show significant oxygen permeation through dense membranes in addition to its good stability and low cost[40]), the concept of increasing the electro-chemical performances of such materials at lower temperature by tuning the anionic nonstoichiometry is attractive and permeation tests will be performed in a further stage. Additionally, it was shown that low-temperature (starting at 600 K) oxygen mobility exists in $SrFeO_{3-x}$ dynamically assisted by lattice instability[41] and possibly leading under topotactique reduction by CaH_2 to the $SrFeO_2$ end-member.[21] It follows that the reduction of the metal lattice by F^- incorporation for O^{2-} should enhance oxygen diffusion through the decrease of the mean chemical bondings, while original diffusion paths are expected in the modified anionic sublattice. Oxygen desintercallation of the title compound is currently under investigation.

■ ASSOCIATED CONTENT

Ⓢ Supporting Information

Details of XRD analysis in situ high temperature of powders, neutron diffraction (ND) profiles of the Rietveld refinement, magnetic structure for $Sr_{0.8}Ba_{0.2}FeF_{0.1}O_{3-\delta}$; additional figures as noted in the text (PDF). This material is available free of charge via the Internet at http://pubs.acs.org

■ AUTHOR INFORMATION

Corresponding Author

*E-mail: olivier.mentre@ensc-lille.fr.

■ ACKNOWLEDGMENTS

The authors are grateful to Florence Porcher (LLB, Saclay, France) for her help in ND data collection. The "Fonds Europeéens de Développement Régional (FEDER)", CNRS, "Région Nord Pas-de-Calais", and "Ministère de l'Education Nationale de l'Enseignement Supérieur et de la Recherche" are acknowledged for fundings of X-ray diffractometers . The Agence Nationale pour la Recherche is thanked for financial support through the MAD-BLAST project ref ANR-09-BLAN-0187-01.

■ REFERENCES

(1) Cussen, E. J.; Battle, P. D. *Chem. Mater.* **2000**, *12*, 831−838.

(2) Adkin, J. J.; Hayward, M. A. *Chem. Mater.* **2007**, *19*, 755−762.

(3) Adkin, J. J.; Hayward, M. A. *J. Solid State Chem.* **2006**, *179*, 70−76.

(4) Hadermann, J.; Abakumov, A. M.; Adkin, J. J.; Hayward, M. A. *J. Am. Chem. Soc.* **2009**, *131*, 10598−1064.

(5) Boulahya, K.; Parras, M.; Gonzalez-Calbet, J. M.; Amador, U.; Martinez, J. L.; Tissen, V.; Fernandez-Diaz, M. T. *Phys. Rev. B* **2005**, *71*, 144402.

(6) Hector, A. L.; Hutchings, J. A.; Needs, R. L.; Thomas, M. F.; Weller, T. *J. Mater. Chem.* **2001**, *11*, 527.

(7) Kauffmann, M.; Mentré, O.; Legris, A.; Tancret, N.; Abraham, F.; Roussel, P. *Chem. Phys. Lett.* **2006**, *432*, 88.

(8) Ehora, G.; Renard, C.; Daviero-Minaud, S.; Mentré, O. *Chem. Mater.* **2007**, *19*, 2924−2926.

(9) Strauss, S. W.; Fankuchen, I.; Ward, R. *J. Am. Chem. Soc.* **1951**, *73*, 5084−5086.

(10) Itoh, T.; Nishida, Y.; Tomita, A.; Fujie, Y.; Kitamura, N.; Idemoto, Y.; Osakac, K.; Hirosawa, I.; Igawad, N. *Solid State Commun.* **2009**, *149*, 41−44.

(11) McIntosh, S.; Vente, J. F.; Haije, W. G.; Blank, D. H. A.; Bouwmeester, H. J. M. *Chem. Mater.* **2006**, *18*, 2187−2193.

(12) Shao, Z.; Haile, S. M. *Nature* **2004**, *431*, 170−173.

(13) McIntosh, S.; Vente, J. F.; Haije, W. G.; Blank, D. H. A.; Bouwmeester, H. J. M. *Solid State Ion.* **2006**, *177*, 1737−1742.

(14) Grenier, J. C.; Wattiaux, A.; Pouchard, M.; Hagenmuller, P.; Parras, M.; Vallet, M.; Calbet, J.; Alario-Franco, M. A. *J. Solid State Chem.* **1989**, *80*, 6−11.

(15) Gonzalez-Calbet, J. M.; Parras, M.; Vallet-Regi, M.; Grenier, J. C. *J. Solid State Chem.* **1990**, *86*, 149−159.

(16) Clemens, O.; Haberkorn, R.; Slater, P. R.; Beck, H. P. *J. Solid State Sci.* **2010**, *12*, 1455−1463.

(17) Heap, R.; Slater, P. R.; Berry, F. J.; Helgason, O.; Wright, A. J. *Solid State Commun.* **2007**, *141*, 467−470.

(18) Berry, F. J.; Ren, X.; Heap, R.; Slater, P.; Thomas, M. F. *J. Phys. Chem. Solids* **2008**, *69*, 2032−2036.

(19) Hodges, J. P.; Short, S.; Jorgensen, J. D.; Xiong, X.; Dabrowski, B.; Mini, S. M.; Kimball, C. W. *J. Solid State Chem.* **2000**, *151*, 190−209.

(20) Schmidt, M.; Campbell, S. J. *J. Solid State Chem.* **2001**, *156*, 292−304.

(21) Tsujimoto, Y.; Tassel, C.; Hayashi, N.; Watanabe, T.; Kageyama, H.; Yoshimura, K.; Takano, M.; Ceretti, M.; Ritter, C.; Paulus, W. *Nature* **2007**, *450*, 1062−1065.

(22) Yamamoto, T.; Li, Z.; Tassel, C.; Hayashi, N.; Takano, M.; Isobe, M.; Ueda, Y.; Ohoyama, K.; Yoshimura, K.; Kobayashi, Y.; Kageyama, H. *Inorg. Chem.* **2010**, *49*, 5957.

(23) Tassel, C.; Pruneda, J. M.; Hayashi, N.; Watanabe, T.; Kitada, A.; Tsujimoto, Y.; Kageyama, H.; Yoshimura, K.; Takano, M.; Nishi, M.; Oyama, K.; Mizumaki, M.; Kawamura, N.; Iniguez, J.; Canadell, E. *J. Am. Chem. Soc.* **2008**, *131*, 221−229.

(24) Seinberg, L.; Yamamoto, T.; Tassel, C; Kobayashi, Y.; Hayashi, N.; Kitada, A.; Sumida, Y.; Watanabe, T.; Nishi, M.; Ohoyama, K.; Yoshimura, K.; Takano, M.; Paulus, W.; Kageyama, H. *Inorg. Chem.* **2011**, *50*, 3982.

(25) Rietveld, H. M. *J. Appl. Crystallogr.* **1969**, *2*, 65.

(26) Carvajal, R. *J. Phys. B* **1993**, *55*, 192 (program Fullprof available from http://www-llb.cea.fr/fullweb/fp2k/fp2k.htm).

(27) Sturza, M.; Daviero-Minaud, S.; Kabbour, H.; Gardoll, O.; Mentré, O. *Chem. Mater.* **2010**, *22*, 6726−6735.

(28) Sturza, M.; Kabbour, H.; Daviero-Minaud, S.; Filimonov, D.; Pokholok, K.; Tiercelin, N.; Porcher, F.; Aldon, L.; Mentre, O. *J. Am. Chem. Soc.* **2011**, *133*, 10901.

(29) Alekseeva, A. M.; Abakumov, A. M.; Rozova, M. G.; Antipov, E. V.; Hadermann, J. *J. Solid State Chem.* **2004**, *170*, 731−738.

(30) Brese, N. E.; O'Keeffe, M. *Acta Crystallogr.* **1991**, *B47*, 192−197.

(31) Goodenough, J. B. *Phys. Rev.* **1955**, *100*, 564.

(32) Kanamori, J. *J. Phys. Chem. Solids* **1959**, *10*, 87.

(33) Helgason, Ö. *Hyperfine Interactions* **2008**, No. 184, 143−146.

(34) Inaguma, Y.; Greneche, J. M.; Crosnier-Lopez, M.-P.; Katsumata, T.; Calage, Y.; Fourquet, J. L. *Chem. Mater.* **2005**, No. 17, 1386−1390.

(35) Berastegui, P.; Eriksson, S.-G.; Hull, S. *Mater. Res. Bull.* **1999**, *34*, 303−314.

(36) Demont, A.; Dyer, M. S.; Sayers, R.; Thomas, M. F.; Tsiamtsouri, M.; Niu, H. N.; Darling, G. R.; Daoud-Aladine, A.; Claridge, J. B.; Rosseinsky, M. J. *Chem. Mater.* **2010**, *22*, 6598−6615.

(37) Mentré, O.; Kabbour, H.; Ehora, G.; Tricot, G.; Daviero-Minaud, S.; Whangbo, M. H. *J. Am. Chem. Soc.* **2010**, *132*, 4865−4875.
(38) Lebon, A.; Adler, P.; Bernhard, C.; Boris, A. V.; Pimenov, A. V.; Maljuk, A.; Lin, C. T.; Ulrich, C.; Keimer, B. *Phys. Rev. Lett.* **2004**, *92*, 037202.
(39) Srinath, S.; Mahesh Kumar, M.; Post, M. L.; Srikanth, H. *Phys. Rev. Lett. B* **2005**, *72*, 054425.
(40) Kida, T.; Takauchi, D.; Watanabe, K.; Yuasa, M.; Shimanoe, K.; Teraoka, Y.; Yamazoe, N. *J. Electrochem. Soc.* **2009**, *156*, E187−E191.
(41) Paulus, W.; Schober, H.; Eibl, S.; Johnson, M.; Berthier, T.; Hernandez, O.; Ceretti, M.; Plazanet, M.; Conder, K.; Lamberti, C. *J. Am. Chem. Soc.* **2008**, *130*, 16080−16085.